Highly anisotropic thermal expansion in molecular films of dicarboxylic fatty acids

Lilach Tamam, Henning Kraack, Eli Sloutskin, Benjamin M. Ocko, and Moshe Deutsch

Phys. Rev. B **85**, 205449 — Published 25 May 2012

DOI: 10.1103/PhysRevB.85.205449

Highly anisotropic thermal expansion in molecular films of dicarboxylic fatty acids

Lilach Tamam,[1,*] Henning Kraack,[1,†] Eli Sloutskin,[1] Benjamin M. Ocko,[2] and Moshe Deutsch[1,‡]

[1] *Physics Dept. & Institute of Nanotechnology, Bar-Ilan University, Ramat-Gan 52900, Israel*
[2] *Condensed Matter Physics & Materials Sciences Department, Brookhaven National Laboratory, Upton NY 11973, USA*

(Dated: May 15, 2012)

Ångström-resolution x-ray measurements reveal the existence of two dimensional crystalline order in molecularly thin films of surface-parallel-oriented fatty diacid molecules supported on a liquid mercury surface. The thermal expansion coefficients along the two unit cell vectors are found to differ seventeen-fold. The high anisotropy of the 2D thermal expansion and the crystalline coherence length are traced to the different bonding in the two direction: van der Waals normal to, and covalent plus hydrogen bonding along the molecular backbone axis. Similarities with, and differences from, negative thermal expansion materials are discussed.

PACS numbers:

Thermal expansion of matter reflects the anharmonicity of the potential binding the constituent molecules[1–4]. When the crystal-binding potential experienced by a molecule is different along different crystalline axes, anisotropic thermal expansion results. As such expansion is a sensitive macroscopic manifestation of the binding potential's properties, structural motifs, and molecular dynamics[3–5], it has been intensively studied both experimentally and theoretically. However, these studies addressed almost exclusively 3D crystals, yielding, among other things, intriguing effects like negative volume expansion, i.e. macroscopic thermal *contraction* with increasing temperature[2,4,6,7]. Very few experimental studies of thermal expansion have been carried out on quasi-2D thin organic films. Of these, ordered Langmuir films (LFs) supported on water[8] or mercury[9–11] are of special interest. Unlike solid-supported films, where the film's binding to the substrate's stationary molecules plays a dominant role in determining the thermal expansion, a liquid support, comprising mobile molecules, minimizes the substrate's interference with the intrinsic behaviour of the film. Liquid-supported organic LFs were found to exhibit either isotropic thermal expansion coefficients for rotator phases[8,9,12] or mildly anisotropic thermal expansion coefficients for herringbone-packed crystalline phase[8,11]. However, in all such films studied to date, the molecules were oriented roughly normal to the film surface, and the lateral interaction was an isotropic van der Waals (vdW) interaction. The anisotropic thermal expansion coefficients in these herringbone-packed layers were due to the anisotropy of the packing, not of the interaction.

We present here a study of the temperature dependence of the structure of fatty diacid LFs on mercury, where the molecules are oriented parallel to the surface. While this seems to be a rather trivial change, it has important consequences. A high thermal expansion anisotropy is now found, and shown to originate in the different interactions along the two lateral crystallographic directions: vdW in one, and hydrogen- and covalent-bonding in the other. The concomitantly different binding stiffness, and consequent difference in the excited vibrational modes along the two directions leads to a 17-fold difference in the thermal expansion coefficients, and a 2-fold difference in the crystalline coherence length, in the two crystallographic directions.

One of the fatty diacid molecule studied is shown in Fig. 1(a). Note the carboxyl endgroups, which allow hydrogen bonding[13] at both ends of the molecule and thus play a dominant role in establishing the in-plane order. The corresponding Wilhelmy-plate measured[9,14] surface pressure(π)/molecular area(A) isotherm is shown in Fig. 1(b). The leveling-off of the curve ($\sim$140 Å^2/molecule) following the steep rise ($\sim$160 Å^2/molecule) marks the point where the surface-parallel molecules of the 2D gas (covering the surface at $A \gg 160$ Å^2/molecule) touch each other and form a densely packed monolayer of surface-parallel molecules[9,12]. Ångström-resolution X-ray reflectivity (XR)[15–17] and grazing incidence diffraction (GID)[15,17] were used to determine, respectively, the surface normal, and surface parallel structure of LFs of fatty diacid molecules of carbon numbers $13 \leq n \leq 22$ for temperatures $5°\text{C} \leq T \leq 25°\text{C}$. As GID intensities are very low for these thin LFs, all x-ray measurements were carried out at the highest density (lowest A), just before film collapse, as shown by the arrow for the example in Fig. 1(b). Since we wish to focus here on the thermal expansion, we discuss below only briefly representative examples of the LFs' structure. A full discussion of the structural details of these LFs and their T and n variation will be published elsewhere[18], and the present experimental details are given in the Supplementary Material.

X-ray reflectivity (XR), the reflected intensity fraction $R(q_z)$ of an x-ray beam impinging on an interface at a grazing incidence angle ϕ, was measured at beamline X22B, NSLS, Brookhaven National Laboratory, USA. Here $q_z = (4\pi/\lambda)\sin\phi$, and $\lambda = 1.5127$ Å is the x-rays' wavelength[15–17]. The LF's surface-normal structure is extracted from the deviations of $R(q_z)$ from the theoretical Fresnel $R_F(q_z)$ of an ideally flat and abrupt interface. The measured $R(q_z)$ (symbols) and ideal $R_F(q_z)$ (dashed line) are shown in Fig. 1(c). $R(q_z)$ is very well reproduced (line) by a fitted box model of the surface-normal electron density $\rho(z)$, employed successfully in previous studies of mercury-

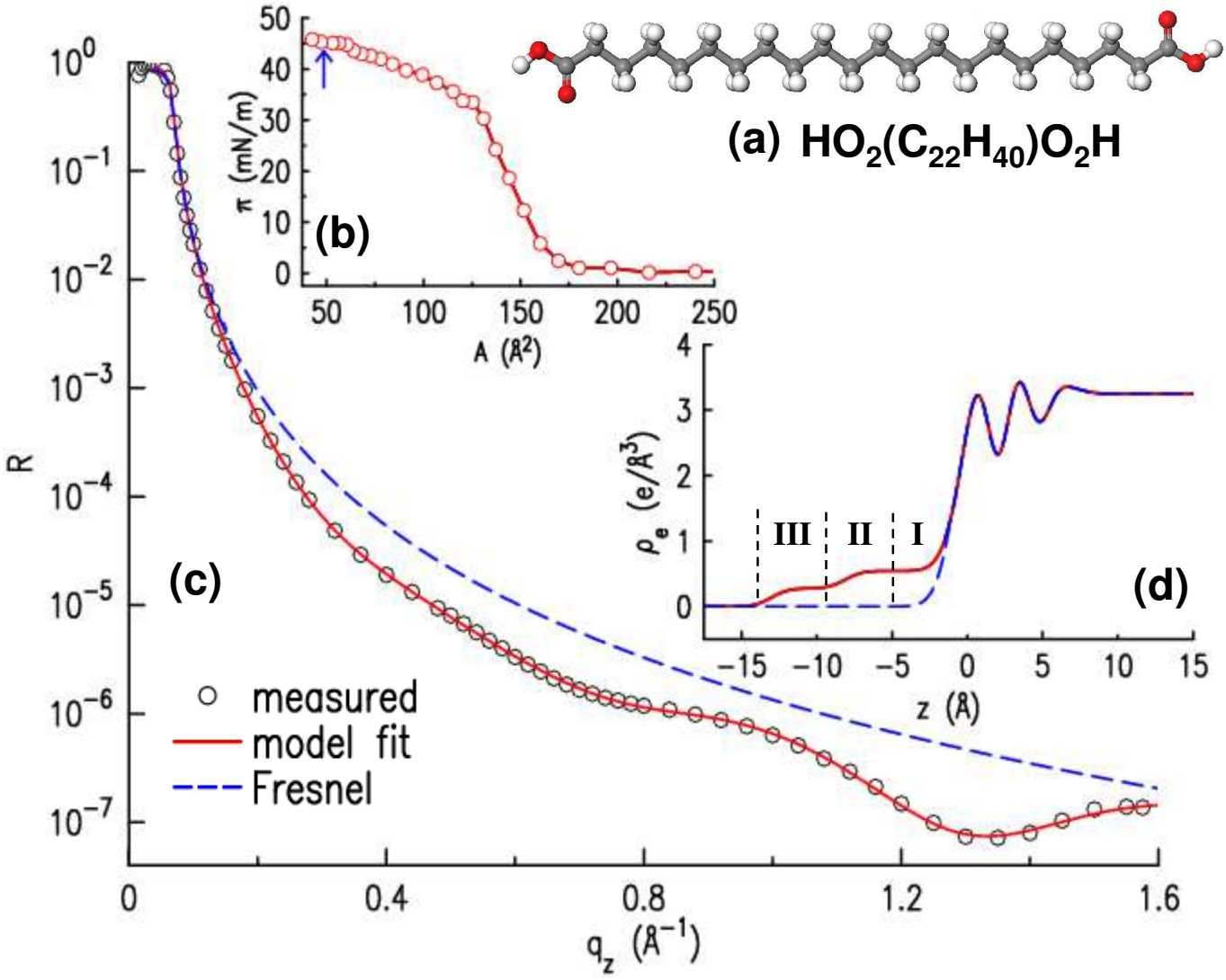

FIG. 1: (Color online) (a) A 22-carbon fatty diacid molecule. Atom color codes: carbon - dark gray, hydrogen - light gray, oxygen - red(dark gray). (b) Surface pressure(π)/molecular area(A) isotherm of the molecule in (a) on mercury. The arrow marks $A \approx 45$ Å^2/molecule, where the XR curve shown in (c) was measured. (c) Measured (symbols) and model-fitted (solid line) XR curve, $R(q_z)$, and the Fresnel XR (dashed line) of an ideally smooth and flat mercury surface. (d) the electron density profile (solid line) derived from the model fit in (c), and the mercury's contribution (dashed line). The vertical dashed lines mark the 3 monolayers of the surface film.

supported organic LFs[9,14,19,20]. It uses 6 slabs to mimic the decaying layering of the mercury near an interface[21,22] plus the minimal number of additional slabs needed to describe the LF. As the XR measurements were carried out at a nominal $A = 45$ Å^2/molecule (arrow in Fig. 1(b)), about a third of the area of a flat-lying molecule, a stack of three monomolecular layers was expected. Indeed, three equal-thickness slabs ($d = 4.6 \pm 0.4$ Å) were needed to reproduce well the measured $R(q_z)$. $\rho(z)$ obtained from the fit is shown in Fig. 1(d), exhibiting a three-layer film ~ 13.5 Å thick over the layered mercury surface. Note the high density of the two bottom layers, suggested below to arise from the inclusion of a mercury atom in the carboxyl-carboxyl bond of the molecules[9,12]. No changes with temperature were detected in the reflectivity within the range studied here, implying that within our resolution no changes occur in the surface-normal structure within this range.

GID measurements were carried out on the same LFs studied by XR. For GID, a shallow incidence angle ϕ is used and the detector is scanned out of the reflection plane by an angle 2θ, to yield a surface-parallel scattering vector $q_\parallel \approx (4\pi/\lambda)\sin\theta$. The measured GID patterns for $n = 13$ and $n = 22$ fatty diacid LFs are shown in Fig. 2. The peaks observed can be grouped in two: the low-$q_\parallel$ peaks, $q_\parallel < 1.2$ Å^{-1} and the high-$q_\parallel$ peaks, $q_\parallel \geq 1.2$ Å^{-1}. In the former group, for each n all peak positions are integer multiples of the lowest-order peak, the position of which is roughly

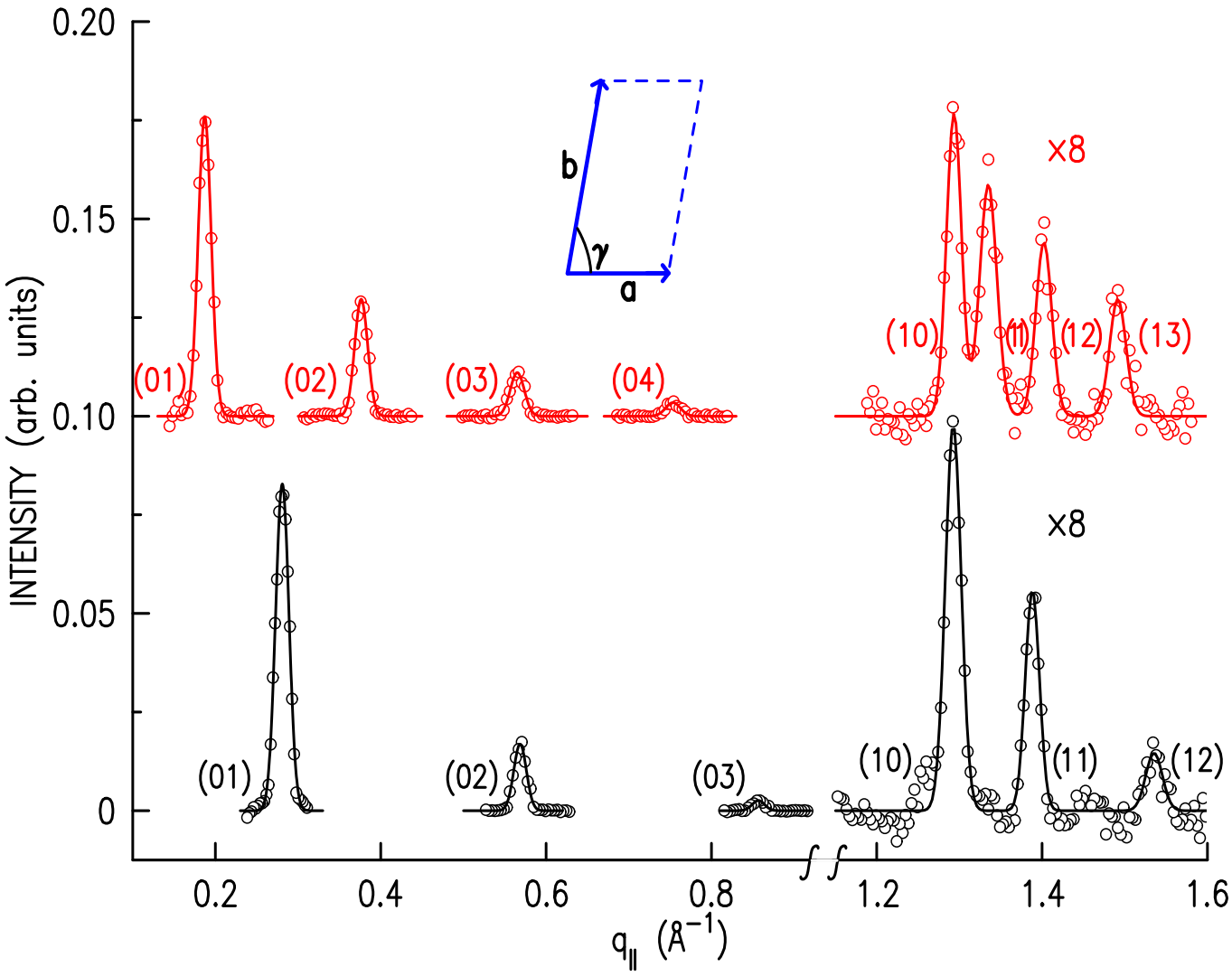

FIG. 2: (Color online) Measured and background subtracted (symbols) GID pattern for 22 carbon (top) and 13 carbon (bottom) diacid film, fitted by a single Gaussian per peak (lines). All peaks are indexed in the oblique 2D unit cell shown. Cell dimensions are given in the text.

inversely proportional to n. In the latter group the first peak, at $q_{\|} \approx 1.3$ Å^{-1}, has the same position for all molecular lengths n. These observations identify the two groups as being associated, respectively, with the length (increasing linearly with n), and width (equal for all n) of the diacid molecule. Indeed, all peaks for all n could be indexed as marked on Fig. 2, using the oblique unit cell shown, with one molecule per cell. For the examples in the figure $\mathbf{a} = 4.95$ Å, $\mathbf{b} = 22.35$ Å, $\gamma = 77°$ for the 13-carbon diacid and $\mathbf{a} = 4.87$ Å, $\mathbf{b} = 33.73$ Å, $\gamma = 83°$ for the 22-carbon diacid. We note in passing that this is the first example of a LF of lying-down molecules to show a full 2D order for such short chain lengths. The only other examples are fatty mono-acid LFs of lengths $n \geq 24$ on mercury[9,12], which however show only a 1D order at room temperature for the diacid lengths $13 \leq n \leq 22$ studied here. The origin of this difference is explained below.

Fig. 3(a) shows the first GID peak, (01) and (10), in each of the two groups discussed above, at two temperatures, for a 17-carbon diacid LF. To allow distinguishing clearly between the curves, we show only the single-Gaussian fit of each, without the measured points. While the (01) peak's position remains almost unchanged upon cooling from 25°C to 5°C, that of the (10) peak is observed to increase significantly (solid black and dashed lines). The thermal expansion coefficients calculated from the peak shifts vs. T for all n studied here are plotted in Fig. 4(a). The thermal expansion coefficient along the **b** axis ($\alpha_{\|}$), reflected in the (01) peak positions, is $\sim$ 17-fold smaller than that perpendicular to it, $\alpha_{\perp}$, reflected in the (10) peak positions. Our $\alpha_{\perp} \approx 3 \times 10^{-4}$ K^{-1} is close to the thermal expansion coefficients of pure-vdW-bound structures, e.g. 2.23×10^{-4} K^{-1} of the R_{II} bulk alkane rotator phase[23],

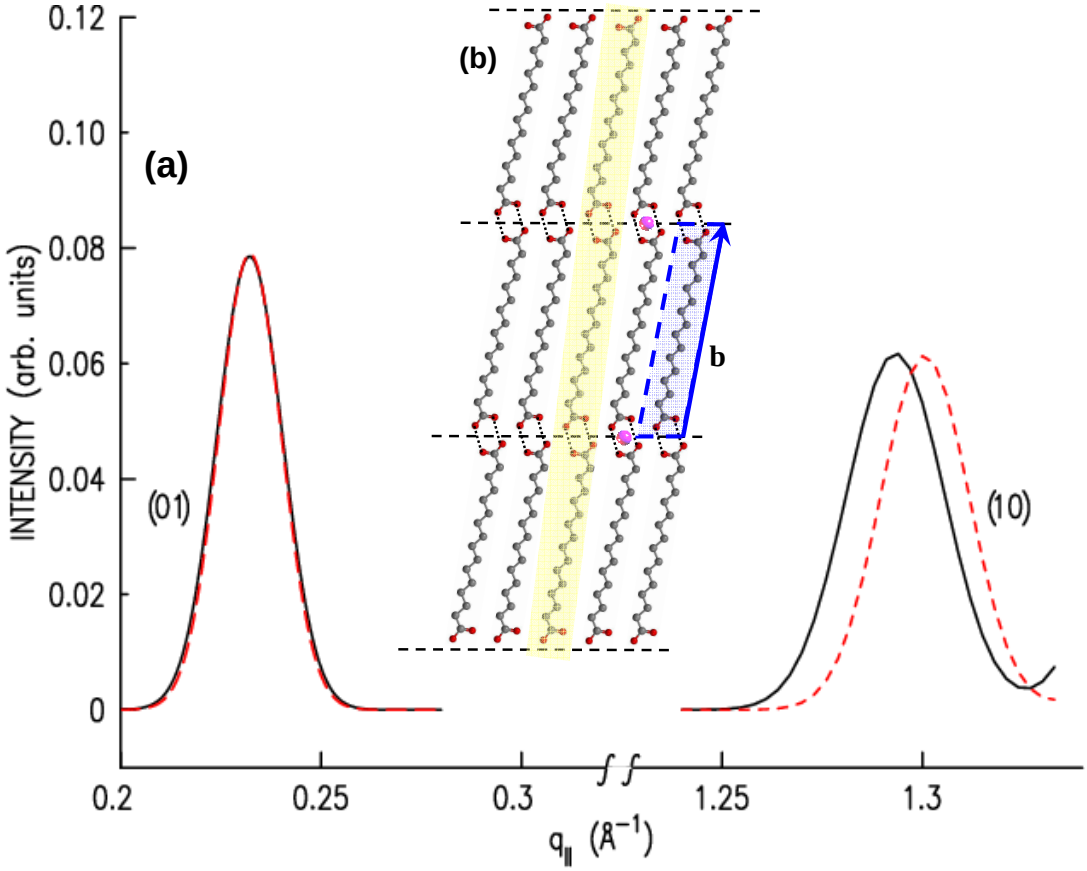

FIG. 3: (Color online)(a) Gaussian fits of the (01) and (10) GID peaks of a 17-carbon diacid film at 25°C (solid line) and at 5°C (dashed line). (b) Schematic top view of the surface-parallel molecular order of a diacid LF. A metal-ligand-complex bonded chain of molecules is highlighted. The unit cell is shown in a dashed line, with the **b** lattice vector marked by an arrow. The Hg atoms included in the metal-ligand bidentate chelate type complexes binding the diacid molecules to each other are shown for one molecule.

and 6.5×10^{-4} K^{-1} and 5×10^{-4} K^{-1} of mercury-supported monolayers of standing-up molecules of alcohols[10] and fatty acids[12], respectively. Thus, the $\alpha_{\perp}$ found here suggests a vdW-dominated bonding in the $\perp$ direction in our LFs. The much smaller $\alpha_{\|} \approx 1.8 \times 10^{-5}$ K^{-1} implies a stronger binding and a stiffer structure in the $\|$ direction. We note that within our T-range and experimental error bars each of the two thermal expansion coefficients seems to be T- and n-independent.

To understand the thermal expansion's anisotropy consider the LF's molecular level structure emerging from the GID results above and the structure of 3D crystals of fatty diacids[24]. The carboxyl endgroups hydrogen-bond the molecules to each other at both ends forming long, polymer-like chains, in which the long axis of each constituent molecule is shifted laterally from that of its neighbour due to the slight azimuthal rotation of the hydrogen bond from the backbone's axis[20,24]. Such a chain is highlighted in Fig. 3(b). The chains are packed side by side, as shown Fig. 3(b), forming lateral stripes of parallel molecules, the edges of which are marked by dashed lines. The parallel packing of the (n-dependent-width) stripes yields the (n-dependent-position) low-$q_{\|}$ peaks of the GID pattern, while the parallel packing of the (n-independent-width) molecules within the stripe yields the (fixed-position) first high-$q_{\|}$ peak, and its neighbours. Note that fatty mono-acid molecules can form only dimers by their single-end carboxyl[9,12], rather than the long chain of molecules made possible by the two-ends carboxyls of the fatty diacid molecules. The additional entropy associated with the dimers' non-bound ends precludes the emergence of 2D order at room temperature for short $n < 24$ molecules, while for diacids 2D order is found already for the shortest molecule studied here, $n = 13$, and most probably even below that.

The slightly oblique 2D unit cell found here (dashed line, Fig. 3(b)) may well result from a longitudinal shift of adjacent molecular chains relative to each other, caused by the repulsion between the carboxyl bonds of adjacent chains. This packing motif is similar to, though not identical with, the packing motif of 3D fatty diacid crystals[24]. In 3D crystals the bonds' repulsion is further relieved by increasing their separation through a $\sim 35°$ rotation of the

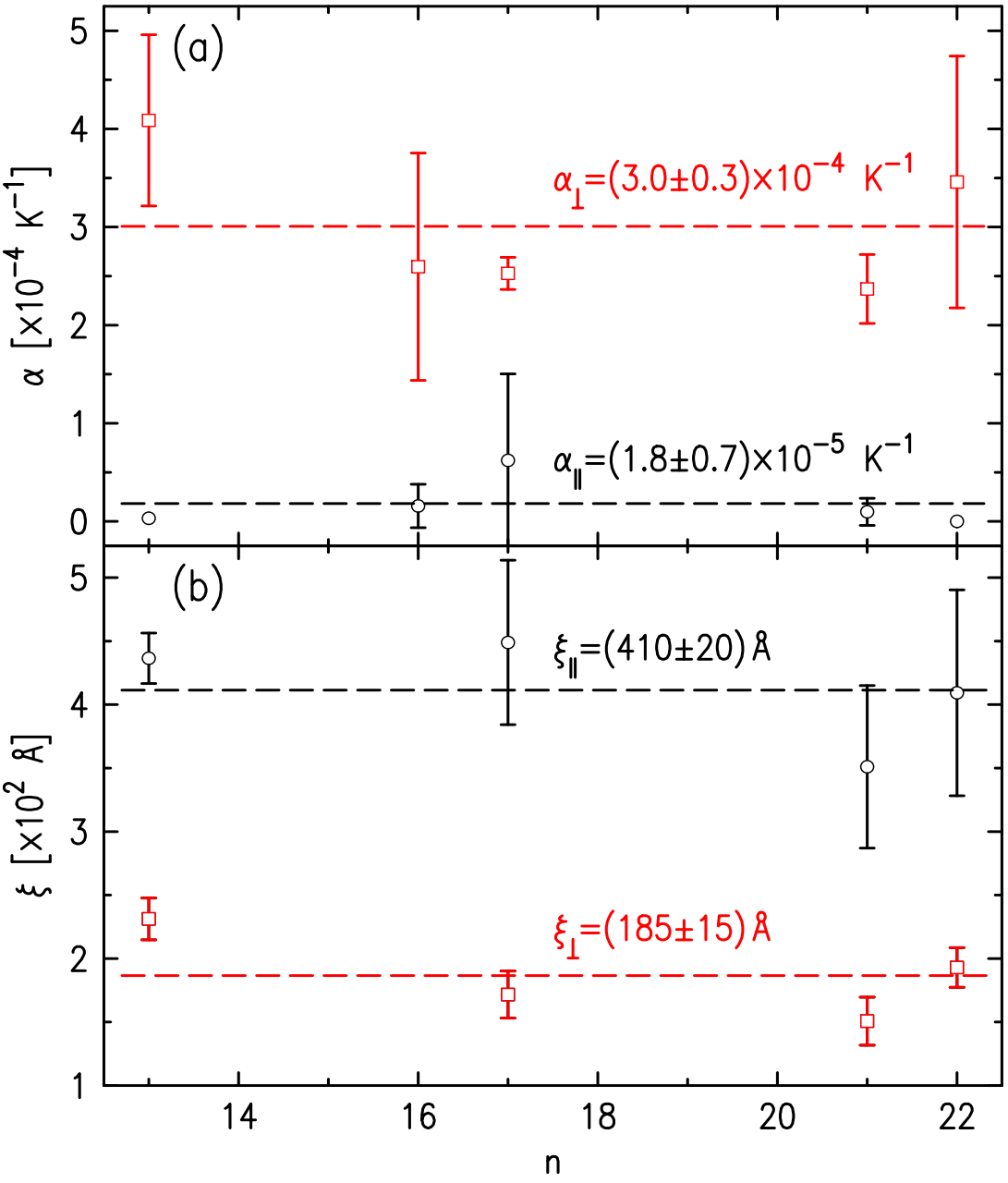

FIG. 4: (Color online)(a) The thermal expansion coefficients parallel ($\alpha_\parallel$) and normal ($\alpha_\perp$) to the crystallographic **b** axis. (b) Coherence lengths of the crystalline domains parallel ($\xi_\parallel$) and perpendicular ($\xi_\perp$) to the crystallographic **b** axis.

chain's backbone plane relative to the average plane containing the chains[24]. A similar rotation of the backbone plane from the surface plane is highly unlikely in our case[20], as it significantly reduces the backbone-mercury contact and thus increases the surface free energy[25]. Indeed, the XR measurements above find a layer thickness of $d = 4.6 \pm 0.4$, corresponding to flat-lying molecules, while 35°-rotated molecules should have yielded a ~ 2.5 Å thicker layer. Another notable difference between the 3D and our 2D crystal structure is that the b-lengths found here exceed for all n the corresponding diacid molecule's length by[18,20] ~ 3 Å. This excess was suggested[9,12,20] to arise from the incorporation of one mercury atom in each carboxyl-carboxyl bond. The elongation's coincidence with the ~ 3.2 Å diameter of the mercury atom[26] supports this suggestion, as does the LFs' ρ being commensurately higher than the pure diacid layer's, as found above in the XR measurements. Our too-sparse GID patterns do not allow to determine the position and coordination nature of the Hg atom included in the carboxyl-carboxyl bond. However, of the four types of metal-ligand complexes identified in the literature[27,28], Cd^{+2} and Pb^{+2} ions exhibit a bidentate chelate bonding motif, where a single metal ion is included in the complex, forming a bond which is partly or fully covalent[27,28]. A similar motif,

shown in Fig. 3(b), is very likely to form for the neighbouring Hg, for which no measurements are available.

The bonding along the chain in Fig. 3(b) consists of covalent bonds among the carbons within each diacid molecule, and a (partly or fully) covalent bond[27,28] of the Hg-carboxyl complex, formed by the inclusion of Hg in the strong resonant-ring-type hydrogen bond, between neighbouring molecules' carboxyls[13,29,30]. The chain-normal purely vdW interaction is much softer. This situation resembles closely, albeit in 2D, the generic structure of 3D crystals of linear (or zigzag) polymers, where the (purely covalent) bonding along the polymer is orders of magnitude stronger than the chain-normal (purely vdW) interaction[2,4,31,32]. The thermal expansion along these directions are related by the Gruneisen theory[4,32] to the various vibrational modes excited in this structure. For a generic polymer, vibrations polarized along the stiffer chain are excited much less than the low frequency modes polarized in the softer, chain-normal direction. The tension effect[4], caused by the chain-normal vibrations, imparts in many polymers a *negative* thermal expansion (i.e. contraction) along the chain and a positive expansion normal to it[4,32]. This effect is found, e.g., in polyethylene, polypropylene and polyoxymethylene[4]. However, unlike in 3D crystals, in mercury-supported LFs some of the main chain-normal vibrations, in particular torsional modes[4,31], are severely hindered by the chains' significant ($\sim$ 45 mJ/m^2, Fig. 1(b)) attraction to the flat surface of the underlying subphase, as discussed in the previous paragraph. This mode inhibition reduces $|\alpha_{\|}|$, as found for mode inhibition due to the presence of inter-chain hydrogen bonds[31], and may also lead to a positive $\alpha_{\|}$. Moreover, if the zigzag polymer is flexible the tension-induced thermal stress can be relieved by a slight change in the C-C bond angle, which was shown to lead to a small but positive $\alpha_{\|}$ in some polymers[32]. Here a similar stress relief may occur by relaxing slightly the length, or chain/bond angle, of the metal-ligand complex, which is much stronger than vdW, but, being not fully covalent, may perhaps be softer than the C-C covalent bonds.

The lateral coherence length of the LF's crystalline domains, ξ, is determined from the Debye-Scherrer formula[33], $\xi \approx 0.9 \times 2\pi/(\Delta^2 q_{\|} - \Delta^2_{res})^{1/2}$, where $\Delta q_{\|}$ is the GID peak's full width at half maximum, and Δ_{res} is the resolution width of the diffractometer. The ξ values in Fig. 4(b) are similar to the $\xi \approx 200$ Å measured for the mercury-supported LF of a poorly-ordering ionic liquid[19], and much smaller than the isotropic $\xi \geq 1000$ Å found for pure-vdW-interacting melt-supported surface-frozen alkane monolayers[15], and mercury-supported LFs of surface-normal fatty acid molecules at area/molecule values just before collapse[12], as is the case here. The reason for the reduced ordering tendency, indicated by the low ξ, is not clear at present. More significantly, Fig. 4(b) demonstrates that the crystalline order persists in our LFs over a distance 2.2 larger along b, the chain direction, than normal to it. This reflects, again, a stronger ordering tendency along the chains due to the strong molecular bonding in this direction as compared to the chain-normal direction, dominated by the softer and weaker vdW interaction.

In conclusion, the molecularly thin films of surface parallel diacid molecules studied here exhibit a fully 2D crystalline order. The thermal expansion is found to be highly anisotropic along the two crystal axes, as is the coherence length of the films' crystalline domains. X-ray measurements reveal that the surface-parallel orientation of the molecules leads to the formation of long, metal-carboxyl-ligand bound chains of diacid molecules, packed parallel to each other, thus yielding a strong covalent bonding along the chain and a softer vdW interaction normal to it. The similarity between this structure and that of generic 3D polymer crystals suggests similar molecular dynamics, which assigns the thermal expansion anisotropy found here to the reduced excitability of thermal vibrational modes polarized along the stiff chains, as compared to those polarized in the softer vdW-bound chain-normal direction. The inhibition of chain-transverse modes by the subphase attraction, and the (limited) flexibility provided by the carboxyl-carboxyl bonds, are suggested to account for the thermal expansion coefficient along the diacid chain being positive here rather than the negative thermal expansion coefficient in 3D polymer crystals. These qualitative suggestions merit quantitative theoretical investigations, which we hope the present study will stimulate.

This work was supported by the US-Israel Binational Science Foundation, Jerusalem. We thank the NSLS, BNL for beamtime at X22B. BNL is supported by DOE contract DE-AC02-76CH0016.

* Present address: Nova Measuring Instruments Ltd., Rehovot, Israel
† Present address: Infineon Technologies AG, Villach, Austria
‡ E-mail:deutsch@mail.biu.ac.il

[1] N. W. Ashcroft and N. D. Mermin, *Solid State Physics* (Holt, Rinehart and Winston, New York, USA, 1976).
[2] W. Miller, C. W. Smith, D. S. Mackenzie, and K. E. Evans, J. Mat. Sci. **44**, 5441 (2009).
[3] T. H. K. Barron, J. G. Collins, and G. K. White, Adv. Phys. **29**, 609 (1980).
[4] G. D. Barrera, J. A. O. Bruno, T. H. K. Barron, and N. L. Allan, J. Phys. Cond Matt. **17**, R217 (2005).
[5] T. G. Gibbons, J. Chem. Phys. **60**, 1094 (1974).
[6] H. Birkedal, D. Schwarzenbach, and P. Pattison, Angew. Chem. Int. Ed. **41**, 754 (2002).
[7] A. D. Fortes, E. Suard, and K. S. Knight, Science **331**, 742 (2011).
[8] V. M. Kaganer, H. Möhwald, and P. Dutta, Rev. Mod. Phys. **71**, 779 (1999).
[9] H. Kraack, B. M. Ocko, P. S. Pershan, and M. Deutsch, Science **298**, 1404 (2002).
[10] H. Kraack, B. M. Ocko, P. S. Pershan, E. Sloutskin, L. Tamam, and M. Deutsch, Langmuir **20**, 5386 (2004).
[11] L. Tamam, H. Kraack, E. Sloutskin, B. M. Ocko, P. S. Pershan, A. Ulman, and M. Deutsch, J. Phys. Chem. B **109**, 12534 (2005).
[12] H. Kraack, B. M. Ocko, P. S. Pershan, E. Sloutskin, L. Tamam, and M. Deutsch, Langmuir **20**, 5375 (2004).
[13] G. R. Desiraju, Acc. Chem. Res. **35**, 565 (2002).
[14] B. M. Ocko, H. Kraack, P. S. Pershan, E. Sloutskin, L. Tamam, and M. Deutsch, Phys. Rev. Lett. **94**, 017802 (2005).
[15] B. M. Ocko, X. Z. Wu, E. B. Sirota, S. K. Sinha, O. Gang, and M. Deutsch, Phys. Rev. E **55**, 3164 (1997).
[16] M. Deutsch and B.M. Ocko, *Encyclopedia of Applied Physics*, vol. 23 (VCH, New York, USA, 1998).
[17] J. Als-Nielsen and D. McMorrow, *Elements of Modern X-ray Physics* (Wiely, New York, USA, 2001).
[18] L. Tamam et al., To be published.
[19] L. Tamam, B. M. Ocko, H. Reichert, and M. Deutsch, Phys. Rev. Lett. **106**, 197801 (2011).
[20] L. Tamam, H. Kraack, E. Sloutskin, and M. Deutsch, J. Phys. Chem. C **115**, 25451 (2011).
[21] A. Elsen, B. M. Murphy, B. M. Ocko, L. Tamam, M. Deutsch, I. Kuzmenko, and O. Magnussen, Phys. Rev. Lett. **104**, 105501 (2010).
[22] L. Tamam, D. Pontoni, T. Hofmann, B. M. Ocko, H. Reichert, and D. M, J. Phys. Chem. Lett. **1**, 1041 (2010).
[23] E. B. Sirota and D. M. Singer, J. Chem. Phys. **101**, 10873 (1994).
[24] V. R. Thalladi, M. Nüsse, and R. Boese, J. Am. Chem. Soc. **122**, 9227 (2000).
[25] S. Xu, S. Yin, H. Liang, C. Wang, L. Wan, and C. Bai, J. Phys. Chem. B **108**, 620 (2004).
[26] J. Emsley, *The Elements* (Oxford University Press, Oxford, UK, 1998), 3rd ed.
[27] W. Dong, R. Wang, G. Mao, and H. Moehwald, Soft Matt. **2**, 686 (2006).
[28] A. Gericke and H. Huhnerfuss, Thin Solid Films **245**, 74 (1994).
[29] T. Steiner, Angew. Chem. Int. Ed. **41**, 48 (2002).
[30] G. R. Desiraju, Angew. Chem. Int. Ed. **46**, 8342 (2007).
[31] R. H. Baughman, J. Chem. Phys. **58**, 2976 (1973).
[32] R. M. Barron, T. H. K. Barron, P. M. Mummery, and M. Sharkey, Can. J. Chem. **66**, 718 (1988).
[33] A. Guinier, *X-Ray Diffraction in Crystals, Imperfect Crystals and Amorphous Bodies* (Freeman, San Francisco, USA, 1963).